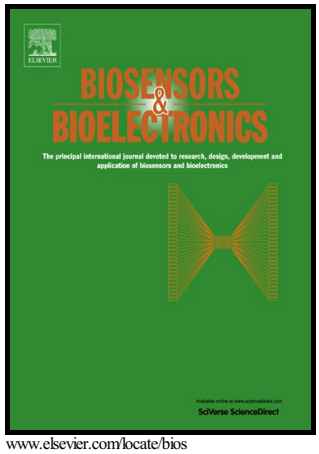

www.elsevier.com/locate/bios

Highly sensitive *Escherichia coli* shear horizontal surface acoustic wave biosensor with silicon dioxide nanostructures

S.T. Ten, U. Hashim, S.C.B. Gopinath, W.W. Liu, K.L. Foo, S.T. Sam, S.F.A. Rahman, C.H. Voon, A.N. Nordin

PII: S0956-5663(16)30925-3
DOI: http://dx.doi.org/10.1016/j.bios.2016.09.035
Reference: BIOS9147

To appear in: *Biosensors and Bioelectronic*

Received date: 18 June 2016
Revised date: 25 August 2016
Accepted date: 10 September 2016

Cite this article as: S.T. Ten, U. Hashim, S.C.B. Gopinath, W.W. Liu, K.L. Foo, S.T. Sam, S.F.A. Rahman, C.H. Voon and A.N. Nordin, Highly sensitive *Escherichia coli* shear horizontal surface acoustic wave biosensor with silico dioxide nanostructures, *Biosensors and Bioelectronic* http://dx.doi.org/10.1016/j.bios.2016.09.035

Highly sensitive *Escherichia coli* shear horizontal surface acoustic wave biosensor with silicon dioxide nanostructures

S.T. Ten[*1,2], U. Hashim[2,3], S.C.B. Gopinath[2,5], W.W. Liu[2], K.L. Foo[2], S.T. Sam[4], S.F.A.Rahman[5], C.H. Voon[2], A.N. Nordin[6]

[1]Malaysian Agricultural Research And Development Institute, Serdang 43400, Malaysia
[2]Institute of Nano Electronic Engineering, Universiti Malaysia Perlis, Kangar 01000, Malaysia,
[3]School of Microelectronic Engineering, Universiti Malaysia Perlis, Arau 02600, Malaysia,
[4]School of Bioprocess Engineering, Universiti Malaysia Perlis, Arau 02600, Malaysia,
[5] Institute of Advanced Technology, Universiti Putra Malaysia, Serdang 43400, Malaysia
[6]Department of Electrical and Computer Engineering, Engineering Faculty, International Islamic University Malaysia, Kuala Lumpur 53100, Malaysia,

ABSTRACT

Surface acoustic wave mediated transductions have been widely used in the sensors and actuators applications. In this study, a shear horizontal surface acoustic wave (SHSAW) was used for the detection of food pathogenic *Escherichia coli* O157:H7 *(E.coli* O157:H7*),* a

dangerous strain among 225 *E. coli* unique serotypes. A few cells of this bacterium are able to cause young children to be most vulnerable to serious complications. Presence of higher than 1 cfu *E .coli* O157:H7 in 25 g of food has been considered as a dangerous level. The SHSAW biosensor was fabricated on 64^0 YX $LiNbO_3$ substrate. Its sensitivity was enhanced by depositing 130 nm thin layer of SiO_2 nanostructures with particle size lesser than 70 nm. The nanostructures act both as a waveguide as well as a physical surface modification of the sensor prior to biomolecular immobilization. A specific DNA sequence from *E. coli* O157:H7 having 22 mers as an amine-terminated probe ssDNA was immobilized on the thin film sensing area through chemical functionalization [$(CHO-(CH_2)_3-CHO)$ and (APTES; $NH_2-(CH_2)_3-Si(OC_2H_5)_3$]. The high-performance of sensor was shown with the specific oligonucleotide target and attained the sensitivity of 0.6439 nM/ 0.1 kHz and detection limit was down to 1.8 femto-molar (1.8×10^{-15} M). Further evidence was provided by specificity analysis using single mismatched and complementary oligonucleotide sequences.

Keywords: E. coli O157:H7, shear horizontal surface acoustic wave (SHSAW), surface functionalization, Deoxyribonucleic acid (DNA), hybridization.

1. Introduction

Escherichia coli (E. coli) bacteria was first discovered in the human colon in 1885 (Feng, Weagant et al. 2002). Most of *E. coli* strains are not only harmless to humans and animal but also act as normal microbiotas that provides mutual benefits with the hosts (Drasar and Hill 1974). However, some strains that have undergone evolutionary changes possess virulence factors to create pathogens (Lim, Yoon et al. 2010). *E. coli* can be divided into at least six different categories based on their pathogenic mechanism, the five most known categories are; enteropathogenic *E. coli* (EPEC), enteroaggregative *E. coli* (EAEC), enteroinvasive *E. coli* (EIEC), enterotoxigenic *E. coli* (ETEC) and enterohemorrhagic *E. coli* (EHEC) (Nataro and Kaper 1998). EHEC produces exotoxins that cause several diseases, from mild diarrhea to fatal hemorrhagic colitis, hemolytic uremic syndrome, and thrombotic thrombocytopenic purpura (Wong, Mooney et al. 2012; Rahal, Kazzi et al. 2014; Goswami, Chen et al. 2015). As recent as 2011, there was an unprecedented outbreak of a highly virulent E. coli strain in Europe that had acquired capabilities of the Shiga toxin (Stx) production (Kieckens, Rybarczyk et al. 2015). Such epidemics result in subsequent food withdrawals from the market and export bans leading to a major negative economic impact (Karch et al., 2012). *E. coli* O157:H7 is easily transmitted through untreated water supply, undercooked or raw meat, milk, fruits, vegetables, food and the use of common facilities, making it easily contagious providing higher probabilities of causing an outbreak (Olsen, Miller et al. 2002; Varma, Greene et al. 2003; Wendel, Johnson et al. 2009; Rahal, Kazzi et al. 2014).

Conventional bacterial detection methods via standard microbiological techniques involve pre-enrichment, selective enrichment, biochemical screening and serological confirmation. All these processes are time consuming (18 to 24 hours or longer) and labor-intensive (Tietjen and

Fung 1995; Hobson, Tothill et al. 1996). Biosensors is a more sensible option for food safety measurements as they are highly sensitive, rapid and provide accurate detection of dangerous pathogens. Recent development have reported dye-based biosensors for enzyme-linked immunosorbent assay (ELISA) (Cho and Irudayaraj 2013), polymerase chain reaction (PCR) (Kim, Singh et al. 2015), and label-free methods using optical detection (Rijal, Leung et al. 2005), surface plasmon resonance (Subramanian, Irudayaraj et al. 2006), potentiometric measurements (Zhou, Yu et al. 2009) and electrochemiluminescent sensors (Leach, Stroot et al. 2010).

Acoustic wave devices is the most promising amongst the variety of label-free sensors due to their ability to obtain the pure mass and viscosity signal of a deposited layer independently (Tsortos, Papadakis et al. 2008; Mitsakakis, Tserepi et al. 2009). The quartz crystal microbalance which employs lamb waves is widely popular for chemical sensing (Sauerbrey 1959). Surface acoustic wave (SAW) devices operate in the range of hundreds of MHz are also popular for both gas and analyte sensing. SAW-based sensors are highly sensitive sensors as the acoustic energy of the acoustic wave is strongly confined at the surface of the device regardless of the thickness of the entire substrate (Grate and Frye 1996). This allows SAW sensors to be very sensitive to surface perturbation and mass loading caused by the binding of the targeted specimen in analyte. "Rayleigh-type" surface acoustic waves (RSAW) are plagued with high losses due to damping (Calabrese, Wohltjen et al. 1987). To counter this, we have proposed the usage of shear horizontal surface acoustic wave device. Particles on the sensing area which are not bound to the surface are detectable but do not dampen the shear acoustic waves in the device (Gammoudi, Tarbague et al. 2010; Zerrouki, Fourati et al. 2010; Hao, Chang et al. 2013).

E. coli O157:H7 is one of the most harmful strains of *E. coli* serotypes. For our work, we have used deoxyribonucleic acid (DNA) based biosensors for effective, selective and sensitive sensing. DNA sensors have higher chemical stability and better ability of distinguishing different closely related strains compared to other bio-recognition elements such as enzymes and antibodies (Teles and Fonseca 2008). To date, most research have been focused to achieve detection at femto molar level (Adzhri, Arshad et al. 2016). In terms of device, previous work on SHSAW biosensors have concentrated on improving device performance by optimizing the sensors' design parameters using Taguchi methods (Tsai, Wu et al. 2009) and adding an adaptive neuro-fuzzy inference system (IANFIS) for signal processing (Tsai, Chiu et al. 2015). Our work intends to improve device performance through the usage of nanostructure waveguides. This has been introduced theoretically by (Zhang 2009) where improvement in the device's performance has been predicted via simulations and finite element modeling. In this

work, SiO_2 nanoparticles were utilized in experiments both to enhance the SHSAW DNA detection sensitivity as well as to act as a waveguide to reduce attenuation.

2. Material and methods

2.1 Materials and reagents

SAW grade Lithium Niobate ($LiNbO_3$) wafers with 64° Rotated Y-cut (PWLN-5R5551) of 1mm $\pm$ 25 μm thickness, with optical polished surface were obtained from Precision Micro-Optics Inc. Lithium niobate was chosen as piezoelectric substrate due to its low insertion loss, very large electromechanical coupling K^2 and high wave propagation velocity (Branch and Brozik 2004; Ten, Hashim et al. 2012). The SAW transducers are fabricated using standard lithography fabrication method. For this process, acetone and aluminum etch 80-15-23-2 solutions were obtained from Mallinckroot Baker, while positive resist (PR1-2000A) was obtained from Futurrex, Inc. and resist developer (RD 6) was obtained from J.T. Baker. To form the waveguide, we sputtered SiO_2 on the SHSAW device. The RF sputtering target was obtained from Stanford Advanced Materials Corporation. For surface modification, ethanol, 3-aminopropyltriethoxysilane (APTES, 99%) and glutaraldehyde were obtained from Sigma-Aldrich. Phosphate buffer saline (PBS) tablets (dissolved in 100 mL of water, containing 137 mM sodium chloride, 2.7 mM potassium chloride, and 10 mM phosphate buffer, pH 7.3-7.5 to make 1 x PBS) were obtained from Amresco, 99.5% All oligonucleotides related to *E. coli* O157:H7 sequences were designed based on the previous research work of Gordilo et al. (Gordillo, Córdoba et al. 2011), and obtained from AIT Biotech. A 22-mer amine terminated probe (Amino- C6GGATGACAAATATCTGCGCTGC3') was synthesized for probe immobilization. For the verification of the sensor's specificity, sensitivity and control of DNA molecule detection, a 22-mer complementary target DNA, (5'GCAGCGCAGATATTTGTCATCC'3), a 22-mer one-base mismatched DNA (5'GCATCGCAGATATTTGTCATCC'3) and a 18-mer non-complementary DNA (5'TCACTACCCACAAAGGTT3') were utilized. All these oligonucleotides (100 μM) were prepared in nuclease-free water obtained from Promega, and used for serial dilutions. All the prepared dilutions were kept frozen. All surface rinsing and cleaning processes used deionized water (DIW) prepared by Millipore Billerica water system.

2.2. Development of SHSAW with SiO_2 nanoparticles waveguide biosensor

A SHSAW biosensor with SiO_2 nanoparticles waveguide was fabricated using standard lithography process commonly used for fabrication of integrated circuits followed by RF

sputtering. Fabrication flow of the SH-SAW biosensor is detailed in Fig. 1. The active sensing area, covered with SiO_2 nanoparticles is 3 x 15 mm and is placed at the center. The overall process for the IDT fabrication of the device was previously reported in (Ten, Hashim et al. 2014). The process is summarized in Fig.1. Briefly, $LiNbO_3$ substrate was cleaned in an ultrasonic bath with Dimethyl Ketone to remove any particles especially after being cut. The Al interdigitated transducers (IDTs) were formed first by thermal evaporation using Auto 306 Vacuum Coater, followed by photolithography to transfer the desired IDT pattern on to substrate (Fig.1(a)). Positive photoresist, PR1-2000A was spin coated on the substrate at 7000 rpm with the acceleration rate 12000 rpm/s for 5 seconds using WS-650MZ-23NPP spin coater. Alignment and exposure of the pattern were done using MIDAS mask aligner, MDA-400M. After development, excess Al was removed using aluminum etch 80-15-23-2 solution (Fig.1(b)). As the final step, protective photoresist layer was removed by dripping Dimethyl Ketone in the spinner with at the speed of 4000 rpm, followed by rinsing using Isopropanol and DI water.

To form the SiO_2 nanoparticles thin film waveguide, the lift-off process was implemented. The same photoresist PR-2000A and steps were used as in the IDT fabrication except that for the soft baking process, the substrate was heated at 50^0C for 20 minutes instead of 105^0C for 60 seconds to drive out the solvent in the photoresist (Fig. 1(c)). This is due to reduce the corrosion effect on the aluminum metal strip (Skrovan, Alfantazi et al. 2009) by increasing the heating time to be certain that the solvent is evacuated from the coated photoresist. After the development process, photoresist at the exposed area in the center was removed by developer RD6. SiO_2 nanoparticles were then deposited using Dressler, VM 1000A RF sputterer (Fig.1(d)). The power was ramped up slowly from 50 W to 150 W for 4 hours under below 10^{-5} Torr vacuum condition. 99.5% SiO_2 from Stanford Advanced Materials Corporation was used as RF sputtering target and placed 15 cm distance away from targets. The compositions of gases used were argon (50 sccm) and oxygen (5 sccm) and with 20 Torr flow pressure. The SiO_2 deposition rate was 0.54 nm/min. Excess photoresist was removed using the same spinning process described above, leaving the SiO_2 nanoparticles thin film waveguide at the center of the device (Fig.1(e)).

2.3. Functionalization SiO_2 nanoparticles thin layer waveguide surface for DNA detection

The most common method to functionalize the SiO_2 surface (Fig. 2) is through silanization process, using self-assembly of alkoxysilane-based linker (one of the types is 3-aminopropyltriethoxysilane) (Shen, Li et al. 2014). This is because the hydroxyl group (OH)

naturally exists on the SiO_2 surface (Rittigstein 2008) (Fig. 2(a)). The SiO_2 nanoparticles waveguide was first cleaned by using oxygen plasma treatment for 10 minutes at 250 W, 100 kPa vacuum conditions and with 300-400 kPa of O_2 flowing pressure. This is to remove organic contamination and also enhance the silanol group on the surface (Shen, Li et al. 2014). The surface was then functionalized by dripping the center sensing area with 6 µl mixture solution of 2% of 3-aminopropyltriethoxysilane (APTES, 99%) in 98% of solution contained ethanol (10%) and DIW (90%) (to activate APTES (Kiernan 1999)). It was then kept in moist condition (>80%) at room temperature for two hours. The alkoxysilane-based linker from APTES mixture reacted with the hydroxyl group on the SiO_2 surface to form a covalent –Si–O–Si– bond (Fig. 2(b)). Next, the surface was rinsed with DIW and heated on a hot plate at 50^0C for 20 minutes. This was to dry the surface as well as to strengthen bonding of alkoxysilane-based linker on the surface. The following step was dripping mixture solution with 2.5% glutaraldehyde in DIW in the center sensing area at room temperature for an hour. Glutaraldehyde (CHO-(CH2)3-CHO) which constitutes two aldehyde groups, was used as a linker to bind the amine terminated DNA to the surface which had just modified to be amine-terminated APTES (Fig. 2(c)). The excess of glutaraldehyde molecules not bound to the surface were removed by rinsing using PBS solution. One end of the aldehyde groups can have interaction with amine-terminated APTES on the surface while the other end was free for further react with amine-terminated probe DNA. At this stage, the surface was covered by –C=O functional group. After that, immobilization with specific receptor for selective detection of a target molecule was done by dripping 10 µM 5'Amino- C6GGATGACAAATATCTGCGCTGC3' (with NH functional group) on the sensing area (Fig. 2. (e)), until it covered the whole area of the center sensing area. It then was placed in the incubator that maintained the temperature at 30^0C with relative humidity of 80% overnight. Finally, it was then rinsed with PBS solution to remove excess unbound DNA probes. The NH functional group at one end of the DNA probe reacts with –C=O functional to form the covalent bonding and subsequently immobilizes the DNA probe on the surface. It is then ready for hybridization process (Fig. 2(e)).

3. Results and discussion

3.1. Device layout and characterization

In this research, SHSAW devices with SiO_2 nanoparticles waveguide were fabricated using CMOS technology process. The SHSAW device consists of input and output transducers (IDTs) as shown in Fig. 3(a). A sinusoidal electrical excitation is triggered via the Input IDT; the transducer then converts the electrical energy into acoustic waves in the piezoelectric lithium niobate layer. The output IDTs detect the travelling acoustic waves and convert it back into

electrical signals. The main parameters of the device are; the pitch or λ, delay line length, L and electrode aperture, W (Fig. 3(a)). The pitch determines the operating frequency of the device and the delay line length, L determines the size of the active area. Both transducers are covered by silicon dioxide nanoparticles that form a waveguide. In this case, the SHSAW biosensor is detecting APTES which is placed at the center of the delay line. The dimensions of the entire device are 3 x 15 mm. Five different SHSAW devices with varying IDT parameters were fabricated and their mass loading sensitivities were compared prior to usage in bio sensing applications. In this work, the IDT parameters were varied as follows, λ = 32 μm and 12 μm; W = 1.376 μm, 2.464 μm and 720 μm; L = 3.904 mm, 7.296 mm and 2.1 mm; Number of IDT pairs 50 and 73. The microscope image of the SHSAW transducers with silicon dioxide microstructures is shown in Fig. 3(b). Inspection of the device was done by high-power microscopy (HPM) (OLYMPUS-BX51) to make sure there is no short circuit between the IDTs. Scanning electron microscopy (SEM) (JEOL JSM-6460LA) was used to observe the size and width of the IDTs. Fig. 3(c) focuses on the IDTs and the inset shows an FESEM image of the IDT and its dimensions. Each IDT has width of ~ 3 μm. The scheme of the whole device is shown in Fig. 3(d), where each set of input and output IDT is connected to probe pads to enable measurements. The synchronous frequency, f_0 = 386 MHz was measured using a Rohde & Schwarz (ZVL) network analyzer. Upon successful fabrication the IDTs are sputtered with a thin layer of SiO_2 nanoparticles. The SiO_2 nanoparticles size and surface roughness were validated by field emission scanning electron microscope (FESEM), Nova Nano 450 and atomic-force microscopy (AFM), (SPA400-SPI3800, Seiko), respectively. Fig. 3(e) shows the AFM image while Fig. 3(f)) shows the FESEM images where it was observed that the SiO_2 nanoparticles have an average diameter of 43 nm, mean average roughness (RMS) value of 0.66 nm which are comparable with reported work by other researchers on bio-functional surface modification. (Dinh, Pascal et al. 2010).

3.2. Characterization of SiO_2 nanoparticles waveguide

Characterization of the SHSAW biosensor SiO_2 nanoparticles waveguide is critical to verify the successful fabrication of the IDTs and its silicon dioxide layer. Affirmation of surface modification layers is done before the oligonucleotides tests. This is to verify that all the elements were successfully immobilized on the sensing surface. The SiO_2 deposition was validated by Energy Dispersive X-ray Spectrometry (EDX) as shown in Fig. 4(a) to examine the purity of SiO_2 deposition by performing elemental analysis. Silicon (Si) and oxygen (O) elements were proven to exist on $LiNbO_3$ substrate by the EDX spectrum just after SiO_2 RF sputtering process. To confirm that the SiO_2 compound is formed on the surface layer, X-ray diffraction

(XRD) using Bruker D2 Phaser was also performed and reported in Fig. 4(b). Further confirmation of the SiO_2 compound was done by XRD with Cu Kα radiation at λ = 1.5406 Å within the range of 18° to 48° operating at 30 kV and 10 mA under room temperature. The results show that the strong diffraction peak at 21.98^0 is ascribed to the (1,0,1) facet of SiO_2, whereas the other peaks at 28.49^0, 36.38^0 and 42.67^0 are ascribed to the (1,1,0), (1,1,2) and (2,0,2) facets of SiO_2, respectively according to the reported ICDD data (card No. 00-039-1425).

The guiding layer of SiO_2 nanoparticles deposited on the device confines the acoustic energy at the near surface to provide high sensitivities. To verify that the 130.5 nm thick silicon dioxide layer effectively acts as a guiding layer for the lithium niobate substrate, insertion loss measurements of the SHSAW device was measured before and after deposition of the silicon dioxide layer. Supplementary Fig. A clearly illustrates reduction in insertion loss (wave propagation loss) when the silicon dioxide layer is present. Decrease in wave propagation loss indicates the efficient guiding of acoustic energy in the deposited layer (Du, Harding et al. 1996).

Affirmation of the surface modification layers for bio-receptor immobilization processes were done by Fourier transform infrared spectroscopy (FTIR) by Perkin Elmer Spectrum 400 spectrometer. IR spectrum (FTIR), which was used to confirm that the surface is functionalized as shown in Fig. 4(c). The IR spectrum of bare $LiNbO_3$ substrate shows the peak at 1410 cm^{-1}, which agrees with previous work conducted by Sreenivasulu et al. (Sreenivasulu, Prasad et al. 2007). This confirms that FTIR can verify the functional group on the surface and some of the substance kinds. The peaks are shown in spectrum of 1090 and 1400-1500 cm^{-1} which verified the existence of SiO_2. The OH peak at 3250-3320 cm^{-1} representing the hydroxyl functional group appeared after the SiO_2 nanoparticles thin film had undergone for oxygen plasma treatment. The peak regions 1550-1640 cm^{-1} and 3120-3300 cm^{-1} are highly characteristic of the NH functional group, after APTES was applied to the surface; this was clearly verified that APTES was successfully attached on the surface. There were two peak regions found at 1720-1740 cm^{-1} and 1450-1470 cm^{-1} after glutaraldehyde is applied which indicate the presence of functional groups of C=O and CH_2, respectively. The experiment verifies that the reaction between the glutaraldehyde and amine-terminated APTES was completed successfully on the surface. The surface was now replaced with aldehyde group (C=O) (Lambert 1987). Amine-terminated ssDNA binding was proven by the presence of peaks at 1100 cm^{-1}, 1150-1640 cm^{-1} and 3250-3500 cm^{-1}, which indicate the appearance of sugar-phosphate backboned, NH bending of the DNA bases and hydrogen bonding, respectively. These FTIR results were in agreement with the previous report by Singh et al. that the DNA probe was successfully immobilized on the sensing area (Singh, Zack et al. 2010).

3.3 Mass loading and device sensitivity

Fig. 3(d) illustrates the basic configuration of a guided SHSAW as a sensor platform. It consists of a SAW delay line with a silicon dioxide overlayer having a lower shear wave velocity. The SiO_2 guiding layer traps the acoustic energy propagating on the surface, reduces propagation velocity and increases the sensitivity of the surface to pertubations. The SHSAW sensor has a transfer function of $T_2(f)$ where $T_{12}(f)$ is the transfer function of an unperturbed SHSAW device and is described below as (1) (Josse, Bender, Cernosek. 2001).

$$T_2(f) = T_{12}(f)e^{-i(\frac{2\pi l}{\lambda})}e^{i(\frac{2\pi\delta l_s}{\lambda})}e^{-\alpha l_s} \qquad (1)$$

In Eq. 1 $\delta=\Delta V/V$ or the fractional velocity change of the SHSAW due to the sensing effect, λ is the wavelength, α is the attenuation coefficient introduced by the waveguide layer, $l_s = L$ is the sensing path length and l is the IDT center-to-center separation.

In our work, shear waves that propagate in the silicon dioxide waveguide layer of 130.5 nm thickness have a shear wave velocity in the of V_M, which is lower than velocity in the piezoelectric substrate (V_{SH}). Sensitivity of the device is captured as surface mechanical pertubations, which can be measured using the fractional change in wave velocity as described below (Josse, Bender, Cernosek. 2001).:

$$\frac{\Delta V}{V} = -\frac{V_{SH}}{4}(\rho h)\left[1-\left(\frac{V_M}{V_{SH}}\right)^2\right]|U_2|^2 \qquad (2)$$

where ρ is the layer mass density, h is the layer thickness and U_2 is the normalized particle velocity displacement amplitude; ρh represents the mass load per unit surface area. Setting $\Delta m=\rho h$, sensitivity of the device to mass loading (S_m) can be described as $\Delta V/V = \Delta f/f$ where

$$S_m = \lim_{\Delta m\to 0}\left(\frac{\Delta f}{f_0}\right)/\Delta m \quad (3)$$

and assuming that the waveguide is a purely elastic and lossless film. In (3) $\Delta f = f - f_0$ where f_0 is the SHSAW device's unloaded operating frequency and f is the operating frequency with load. In accordance with (2), sensitivity increases as U_2 or the velocity of the film increases, which also indicates that the acoustic energy is trapped to the sensing surface. For viscoelastic films such as the waveguide layer and biochemically sensitive layer, ΔV is a function of shear viscosity coefficient and angular frequency (Josse, Bender, Cernosek. 2001). In our work, the SiO_2 waveguide is assumed to be a low-loss surface as the thickness of the waveguide layer is much less that the SHSAW device pitch or $h << \lambda$ (Josse, Bender, Cernosek. 2001). Equation (3) is sufficient to approximate mass sensitivity of the device as the biolayer consisting of the receptors and the bound antigen is in the order of a few molecules thick, giving a negligible contribution to the sensor's response. In cases where a chemically sensitive and lossy polymer

is deposited on the waveguide layer, the mechanical quality factor (Q) of the device will dictate the device's mass sensitivity. For SAW delay lines, Q is a function of group delay multiplied by the device's operating frequency (Mauder, 1995).

The device's sensitivity to mass loading for the SHSAW sensors can also be quantified in another form using Sauerbrey's equation (Sauerbrey 1959) where $\Delta m=\rho h$:

$$\Delta f = -2\Delta m f_o^2 / A\sqrt{\mu\rho} \quad (4)$$

where f_0 is synchronous frequency, Δf is the frequency change or shift, Δm is the mass added, A is the sensing area, μ and ρ are the shear modulus and the density of the quartz substrate respectively. In relation to our experiment, when the target DNA is trapped by the receptor (DNA probe) immobilized on SiO_2 nanoparticles sensitive layer, mass is added (mass loading effect) on the sensing surface and this consequents the decrease of frequency (indicated by the negative sign in (4)).

The relationship between the f_o, wave propagation velocity, V_{SH} and λ is:

$$f_o = \frac{V_{SH}}{\lambda} \quad (5)$$

Thus more sensitive acoustic based sensors can be produced by increasing f_o (Rodriguez-Madrid, Iriarte et al. 2012) and reducing the IDT's λ according to (5).

In our experiments, as specified in Section 3.1, five different IDT parameters were fabricated; four of them were λ=32 μm (with the average of f_0 = 144.303 MHz) with different delay line length and aperture sizes and one λ=12 μm (with f_0 = 384.948 MHz). Mass loading sensitivities of each device were characterized using photoresist before advancing to the bio-sensing tests. 1mm^2 sensing area was used for this research. In this pre-biosensing test, photoresist PR-2000A was deposited on the center of the sensing area of the 5 devices and the Δf was measured. Photoresist was used as it can stick very firmly on the device's surface.

Measurements for the pre-biosensing test is recorded in Supplementary Fig. B. Devices with larger λ (λ = 32 μm) have lower sensitivities compared to (λ = 12 μm) as shown in Fig. B(a). For devices with the same λ and aperture width (W = 1.376 mm), mass sensitivity is inversely proportional to the delay length (L), where the mass sensitivity is increased from 25.64 MHz/mg to 32.42 MHz/mg with the decrease of delay line length (from 7.296 mm to 3.904 mm). The same trend was observed for (W=2.464 mm) where mass sensitivity increased from 6.15

MHz/mg to 16.32 MHz/mg with the decrease of delay line length. This can be explained based on (1), where the sensor's transfer function $T_2(f)$ is inversely proportional to the delay length, L or l_s. On the other hand, the mass loading sensitivity was also increased with the decrease in aperture size W (from 2.464 mm to 1.376 mm) when all other parameters remain same. Although having a larger W usually translates in providing the sensor's transducers with more input power, having a W that is too large causes the SHSAW device to be lossy as the resistance of the transducers increase with increase in length of the aperture. In this case, W=1.376 mm is found to be the optimum aperture width as it balances resistivity of the transducers with transmission of input power. Amongst the four devices with λ=32 μm, the one with the smaller aperture size (1.376 mm) and shorter delay line length (3.904 mm) is most sensitive with sensitivities of of 32.42 MHz/mg. Reduction in λ provides even higher sensitivities. Our smallest device with λ =12 μm with f_0 = 384.948 MHz, and even smaller aperture size, W=0.72 mm and delay length, L=2.1 mm results in the highest sensitivity of 155.80 MHz/mg (4.8-fold higher than the most sensitive λ =32 μm). This is in agreement with (1)-(5) where shorter delay lengths, smaller λs and optimized W provide more sensitive devices.

3.4. Performance of SiO_2 nanoparticles waveguide biosensors

For the biological experiments, two devices (λ =32 μm; L = 3.904 mm; W= 1.376 mm) and (λ =12 μm; L = 2.1 mm; W= 0.72 mm) were selected for the complementary DNA testing. Both devices underwent the surface modification process specified in Section 2.3 and then were tested with 10 μM and 1 μM concentrations of complementary target DNA. For each test, 5 μl of the complementary target DNA was dropped on the sensing area and then the devices were placed in an incubator to maintain its temperature at 30^0C with relative humidity at 80% for an hour. After that, the devices were rinsed with PBS solution and blow dried before the frequency measurements were taken by using the network analyzer. Dip-dry method was used rather than the submerge method or liquid phase flow-through method. This is because the dip-and-dry method produces larger variation of output response and provides a wider range of concentration measurement (Berkenpas, Millard et al. 2006). The results are graphed in Supplementary Fig. B(b) where that the smaller device with (λ =12 μm) is more sensitive (3.6 times more sensitive than 32 μm pitch size). This trend matches the previous experiment with photoresist which found that λ =12 μm is more sensitive. Fig. B(b) also shows that change in frequency, Δf increases with increase in DNA concentration, indicating that the SHSAW sensor is also sensitive to mass changes.

Further tests were conducted on the device with λ =12 μm to determine the sensor's sensitivity, limit of detection (LOD), specificity and to evaluate the analytical performance as a SiO_2 nanoparticles waveguide SHSAW biosensor. The results of these experiments are shown in Fig. 5. The device sensitivity test was performed by concentration-dependent frequency shift, Δf upon hybridization to the complementary target DNA. The effect of different concentrations of fully complementary target *E. coli* O157:H7, ranging from 0.25 fM to 10 μM were analyzed. The Δf characteristics were plotted as shown in Fig. 5(a), which demonstrates increased Δf with increase in target DNA concentration. As the target DNA concentration increased, there was denser DNA hybridization on the surface which consequents the increased mass loading effect and agrees with (4). The sensor's sensitivity is 0.6439 nM/ 0.1 kHz which was calculated from the slope of the calibration curve. Other than sensitivity, it is important to know limit of detection (LOD), or the lowest concentration of target DNA in an analyte detectable by the sensor. These can be done by calculating the relative change in the f_0 shift of the device to various concentrations of the *E. coli* O157: H7 DNA, a calibration curve (the relative changes in f_0 shift were found to be proportional to the logarithm of *E. coli* O157: H7 DNA concentration) and was plotted as shown in Fig. 6(b). The LOD was calculated using the following equation:

$$Y_{LOD} = Y_{(baseline,immobilization)} + 3\sigma \quad (6)$$

where the σ is the standard deviation of the calibration curve regression, and $Y_{(baseline,immobilization)}$ is assumed as 0, the response signal for blank signal (Hubaux and Vos 1970; Miller 1991). The LOD was then calculated from the calibration curve (Hashim, Arshad et al. 2016). The LOD for this device was found to be 1.8 fM.

Next, specificity tests were conducted using the SHSAW biosensor. To perform this three separate tests were conducted using three separate devices with λ =12 μm; where the first hybridized full complementary target DNA, the second test used one base mismatched target DNA and the third test acts as a control with non-complementary target DNA. Concentration was fixed for all test at 1 μM. Figure 5(C) portrays significant differences in Δf values for each DNA hybridization process. Upon hybridization with fully complementary target DNA and one base mismatched target DNA, the Δf values of 1.5946 MHz and 0.3042 MHz were obtained, respectively. However, very minimal Δf of 0.0392 MHz was recorded for the non-complementary target DNA. The magnitudes of Δf values indicates that the sensor produces large Δf for the specific binding of target DNA with the immobilized probe compared to a low Δf for improper binding with mismatched DNA target. A very low Δf or close to no mass loading

effect is recorded for non-complementary target DNA bindings with the immobilized probe. These show that this DNA biosensor is specific and can discriminate among fully complementary, one base mismatched and non-complementary nucleotides sequences. Supplementary Table 1 compares our research with reported research on acoustic-wave based biosensors used for *E.coli* O157:H7 detection. This SHSAW with SiO_2 nanoparticles waveguide device can be considered as competent biosensor with the sensitivity of 0.6439 nM/0.1 kHz (16.76 pg/0.1 kHz was calculated based on the target complementary DNA molecular weight (MW), 6710 g and with the 5 µl testing volume).

The regeneration or reuse of the biosensor (same device) can be done by denaturing and removing the hybridized *E. coli* O157:H7 target DNA from the surface to regain the original condition with probe immobilized surface. This de-hybridization or denature process was implemented by dropping 10 µl 0f 0.1 M NaOH liquid (Nadzirah, Azizah et al. 2015) on the sensing area for 10 minutes in room temperature and then rinsed with PBS solution and blew to dry. The f_0 of the device were monitored to be back to the values at probe condition before target DNA hybridization process. Three regeneration cycles were done on the same device and a low relative standard deviation (RSD) of 0.06% was obtained indicating good reusability of the SHSAW SiO_2 biosensor.

The reproducibility and repeatability tests were also conducted for the SHSAW SiO_2 biosensor and is summarized in Supplementary Table 2. The reproducibility test was also conducted using two different devices (Device A and Device B) were tested using 2 different concentrations (10 fM and 0.25 fM) and its Δf was recorded, similar to (Hashim, Arshad et al. 2016). The tests were conducted in triplicates for each concentration and RSD of 9.38% and 8.84% were obtained for 10 fM and 0.25 fM respectively indicating good reproducibility.

4. Conclusion

We have presented a novel SHSAW biosensor with silicon dioxide nanostructure waveguide for detection of *E. coli* O157:H7. This biosensor had been thoroughly investigated by analyzing the frequency shifts in response to different concentrations of *E. coli* O157:H7 oligonucleotides. A specific DNA sequence from *E. coli* O157:H7 having 22 mers as an amine-terminated probe ssDNA was immobilized on the thin film sensing area through chemical functionalization [(CHO-$(CH_2)_3$-CHO) and (APTES; NH_2-$(CH_2)_3$-$Si(OC_2H_5)_3$]. The high-performance of sensor was shown to be specific to the oligonucleotide target and attained the sensitivity of 0.6439 nM/ 0.1 kHz and detection limit was down to 1.8 femto-molar (1.8×10^{-15} M). The SHSAW SiO2 biosensor

also demonstrated high specificity, repeatability and reproducibility with RSD values of lower than 10%.

Acknowledgments

This research was supported by Nanofund (RM-5022NF10) from Ministry of Science Technology and Innovation (MOSTI) Malaysia. The authors would like to thank all team members of the Institute of Nano Electronic Engineering, Universiti Malaysia Perlis (UniMAP) and Malaysian Agriculture Research and Development Institute for their technical support and contributions.

References

References

Adam, T. and Hashim,U., 2015. Biosensors and Bioelectronics. 67, 656-661.
Adzhri, R., Arshad, MK.Md., Gopinath, S. C.B, Ruslinda, A.R., Fathil, M.F.M., Ayub, R.M., Nor, M Nuzaihan Mohd, Voon, C.H., 2016. Analytica chimica acta 917, 1-18.
Berkenpas, E., Millard,P., Da Cunha, M.P., 2006. Biosensors and Bioelectronics. 21(12), 2255-2262.
Branch, D. W. and S. M. Brozik , 2004. Biosensors and Bioelectronics. 19(8), 849-859.
Calabrese, G. S., Wohltjen,H., Roy, M. k., 1987. Analytical chemistry. 59(6), 833-837.
Cho, I.-H. and J. Irudayaraj ,2013. International journal of food microbiology 164(1): 70-75.
Dinh, D. H., Pascal, É., Vellutini, L., Bennetau, B., Rebière, D., Dejous, C., Moynet, D., Belin, C., Pillot, J-P., 2010. Sensors and Actuators B: Chemical. 146(1), 289-296.
Drasar, B. S. and Hill, M. J., 1974. Academic Press (London) Ltd., 24/28 Oval Road, London, NWI.
Du, J., Harding, G., Ogilvy, J., Dencher, P., & Lake, M., 1996. Sensors and Actuators A: Physical, 56(3), 211-219.
Dufva, M., 2005. Biomolecular engineering. 22(5), 173-184.
Feng, P., Weagant, S. D., Grant, M.A., Burkhardt, W., Shellfish, M., Water, B., 2002. Bacteriological analytical manual [Monograph on the internet]. US Food and Drugs Administration.
Frenzen, P. D., Drake A., Angulo, F.J., 2005. Journal of Food Protection®. 68(12), 2623-2630.
Freudenberg, J., Schelle, S., Beck, K., Von Schickfus, M., & Hunklinger, S., 1999. Biosensors and Bioelectronics, 14(4), 423-425.
Gammoudi, I., Tarbague, H., Othmane, A., Moynet, D., Rebière, D., Kalfat, R., Dejous, C., 2010. Biosensors and Bioelectronics. 26(4), 1723-1726.
Gizeli, E., Bender, F., Rasmusson, A., Saha, K., Josse, F., Cernosek, R., 2003. Biosensors and Bioelectronics. 18(11), 1399-1406.
Göpel, W., Jones, T. A., Kleitz, M., Lundström, I., Seiyama, T. 2008. Sensors, Chemical and Biochemical Sensors, Wiley.
Gordillo, R., Córdoba, J. J., Andrade, M.J., Luque, M.I., Rodríguez, M., 2011. Meat science. 88(4), 767-773.
Goswami, K., Chen, C., Xiaoli, L., Eaton, K.A., Dudley, E.G., 2015. Infection and immunity. 83(11), 4185-4193.
Grate, J. W. and Frye, G. C. ,1996. Sensors update. 2(1), 37-83.
Hao, H.-C., Chang, H.-Y., Wang, T.-P., Yao, D.-J., 2013. Journal of laboratory automation. 18(1), 69-76.
Hashim, U., Arshad MK. Md., Kasjoo, S., Rahman, S.F.A., Ruslinda, A.R., Fathil, M.F.M., Adzhri, R., Shahimin, M.M., 2016. Biosensors and Bioelectronics. 83, 106-114.

Hickemell, F., Knuth, H., Dablemont, R., Hickernell, T., 1995. IEEE Ultrasonics Symposium, 345-348.
Hobson, N.S., Tothill, I., Turner, A.P.F., 1996. Biosensors and Bioelectronics. 11(5), 455-477.
Howe, E. and Harding, G., 2000. Biosensors and Bioelectronics. 15(11), 641-649.
Huang, I.-Y., Lin, C.-Y., Sun, C.-H., 2011. IEEE Sensors, 488-491.
Hubaux, A., Vos, G., 1970. Analytical chemistry, 42(8), 849-855.
Josse, F., Bender, F., and Cernosek, R. W., 2001. Analytical Chemistry, 73(24), 5937-5944.
Karch, H., Strockbine, N., OBrien, A., 1986. FEMS Microbiol. Lett. 35, 141–145.
Kieckens, E., Rybarczyk, J., Barth, S. A., Menge, C., Cox, E., 2015. Veterinary Microbiology.
Kiernan, J., 1999. Microscopy Today: 99-96.
Kim, K.-P., Singh, A.K., Bai, X., Leprun, L., Bhunia, A.K., 2015. Sensors 15(9): 22672-22691.
Lambert, J. B. , 1987. Introduction to organic spectroscopy.
Leach, K. M., Stroot, J. M., Lim, D.V., 2010. Applied and Environmental Microbiology. 76(24), 8044-8052.
Lim, J. Y., Yoon J. W., Hovde, C.J., 2010. Journal of microbiology and biotechnology. 20(1), 5.
Mauder, A., 1995. Sensors and Actuators B, 26-27, 187-190.
Mitsakakis, K., Tserepi A., Gizeli, E. 2009. Microelectronic Engineering. 86(4), 1416-1418.
Nadzirah, S., Azizah, N., Hashim, U., Gopinath, S.C.B., Kashif, M., 2015. PloS one. 10(10), e0139766.
Nataro, J. P. and Kaper, J. B., 1998. Clinical microbiology reviews. 11(1), 142-201.
Ngo, V. K. T., Nguyen D. G., Nguyen, H.P.U., Nguyen, T.K.M, Huynh, T.P., Lam, Q.V., Huynh, T.D., Truong, T.N.L., 2014. Advances in Natural Sciences: Nanoscience and Nanotechnology. 5(4), 045004.
Olsen, S. J., Miller, G., Breuer, T., Kennedy, M., Higgins, C., Walford, J., McKee, G., Fox, K., Bibb, W., Mead, P., 2002. Emerging infectious diseases. 8(4), 370-375.
Rahal, E. A., Kazzi, N., Nassar, F.J., Matar, G.M., 2014. Shiga toxin-producing Escherichia coli in human, cattle and foods. Strategies for detection and control. 30.
Rijal, K., Leung A., Shankar, P.M., Mutharasan, R., 2005. Biosensors and Bioelectronics. 21(6), 871-880.
Rittigstein, P., 2008. The Glass Transition and Physical Aging Behavior of Polymer Nanocomposites Studied Via Fluorescence, Northwestern University.
Rodriguez-Madrid, J., Iriarte, G.F., Pedros, J., Williams, O.A., Brink, D., Calle, F., 2012. Electron Device Letters, IEEE. 33(4), 495-497.
Sauerbrey, G. 1959. Z. Phys. 155(2), 206-222.
Shen, M.-Y., Li B.-R., Li, Y.-K., 2014. Biosensors and Bioelectronics. 60, 101-111.
Singh, S., Zack, J., Kumar, D., Srivastava, S.K., Saluja, D., Khan, M.A., Singh, P.K., 2010. Thin Solid Films. 519(3), 1151-1155.
Skrovan, J., Alfantazi, A., Troczynski, T., 2009. Journal of applied electrochemistry. 39(10), 1695-1702.
Sreenivasulu, A., Prasad, T.N.V.K.V, Buddhudu, S., 2007. Indian Journal of Pure and Applied Physics. 45(9), 741.
Su, X.-L. and Li, Y., 2004. Biosensors and Bioelectronics. 19(6), 563-574.
Subramanian, A., Irudayaraj, J., Ryan, T., 2006. Biosensors and Bioelectronics. 21(7), 998-1006.
Teles, F. and Fonseca, L., 2008. Talanta. 77(2), 606-623.
Ten, S.T., Hashim, U., Malek, F., Liu, W.W., Foo, K.L., Voon, C.H., Wee, F.H., Lee, Y.S., Hisham, H., Sudin, A., 2014. Semiconductor Electronics (ICSE), IEEE International Conference on, IEEE.
Ten, S.T., Hashim U., Sudin, A., Liu, W.W., Salleh, N.H.M., Nazwa, T., 2012. Biomedical Engineering and Sciences (IECBES), IEEE EMBS Conference on, IEEE.
Tietjen, M. and Fung, D. Y., 1995. Critical reviews in microbiology. 21(1), 53-83.
Tsai, H.-H., Wu, D. H., Chiang, T.-L., Chen, H.H., 2009. Sensors. 9(3), 1394-1408.
Tsai, J.-T., Chiu K.-Y., Chou, J.-H., 2015. Access, IEEE. 3, 1614-1619.
Tsortos, A., Papadakis, G., Mitsakakis, K., Melzak, K.A., Gizeli, E., 2008. Biophysical journal. 94(7), 2706-2715.

Varma, J. K., Greene, K. D., Reller, M.E., DeLong, S.M., Trottier, J., Nowicki, S.F., DiOrio, M., Koch, E.M., Bannerman, T.L., York, S.T., 2003. Jama . 290(20), 2709-2712.
Wendel, A. M., Johnson, D. H., Sharapov, U., Grant, J., Archer, J.R., Monson, T., Koschmann, C., Davis, J.P., 2009. Clinical infectious diseases. 48(8), 1079-1086.
Wong, C. S., Mooney, J. C., Brandt, J.R., Staples, A.O., Jelacic, S., Boster, D.R., Watkins, S.L., Tarr, P.I., 2012. Clinical infectious diseases. 55(1), 33-41.
Zerrouki, C., Fourati, N., Lucas, R., Vergnaud, J., Fougnion, J.-M., Zerrouki, R., Pernelle, C., 2010. Biosensors and Bioelectronics. 26(4), 1759-1762.
Zhang, G., 2009. Journal of Sensors.
Zhou, Y., Yu, B., Guiseppi-Elie, A., Sergeyev, V., Levon, K., 2009. Biosensors and Bioelectronics .24(11), 3275-3280.

Legends

Fig. 1. Shear Horizontal Surface Acoustic Wave device with SiO_2 nanoparticles waveguide fabrication flow.(a) Aluminium deposition using thermal evaporation, (b) Patterning the Al transducers using lithography, (c) defining the active area using photoresist (d) SiO2 deposition using RF sputtering (d) Patterning the SiO2 layer using lift-off process

Fig. 2. The surface functionalization process including the surface modification steps from (a) SiO_2 deposition, (b) APTES, (c) glutaraldehyde to (d) probe DNA immobilization processes and (e) DNA hybridization process on $LiNbO_3$ substrate.

Fig. 3. SHSAW biosensor with SiO_2 nanoparticles waveguide. Clockwise from top left (a) The IDT design parameters (b) Microscope image of the SHSAW fabricated biosensor for *E. coli* O157:H7 detection with APTES. (c) HPM and SEM images of the IDTs. (d) Microscope image of the whole SHSAW biosensor and probe pads. (e) AFM image of deposited SiO_2 layer. (f)FESEM image of the SiO_2 nanoparticles at 5 kV with 800,000 magnification.

Fig. 4. Affirmation of surface functionalization layers: (a) EDX spectrum upon SiO_2 deposition. (b) SiO_2 compound confirmation by XRD. (c) Infrared spectrum scanning by FTIR upon every layer of surface modification process.

Fig. 5. Analytical performance of SiO_2 nanoparticles waveguide SHSAW biosensor: (a) Frequency shift response curve with different concentrations of *E. coli* O157:H7 DNA. (b) Calibration curve of the relative change in frequency shift according to different concentrations of *E. coli* O157:H7 DNA, display limit of detection (LOD). (c) Hybridization specificity demonstrated by the frequency shift to the complementary, one base mismatched and non-complementary DNA sequences.

Highlights

- SHSAW biosensor with nanostructure waveguide and specific DNA receptor is developed.
- Improved sensitivity by manipulation of IDT parameters is discussed.
- Amine and aldehyde based chemical binding method for DNA immobilization is discussed.
- Mass-sensing of *E. coli* O157:H7 DNA via frequency detection is discussed.
- High sensitivity of 0.6439 nM/0.1 KHz, low LOD of 1.8 fM concentration is reported.

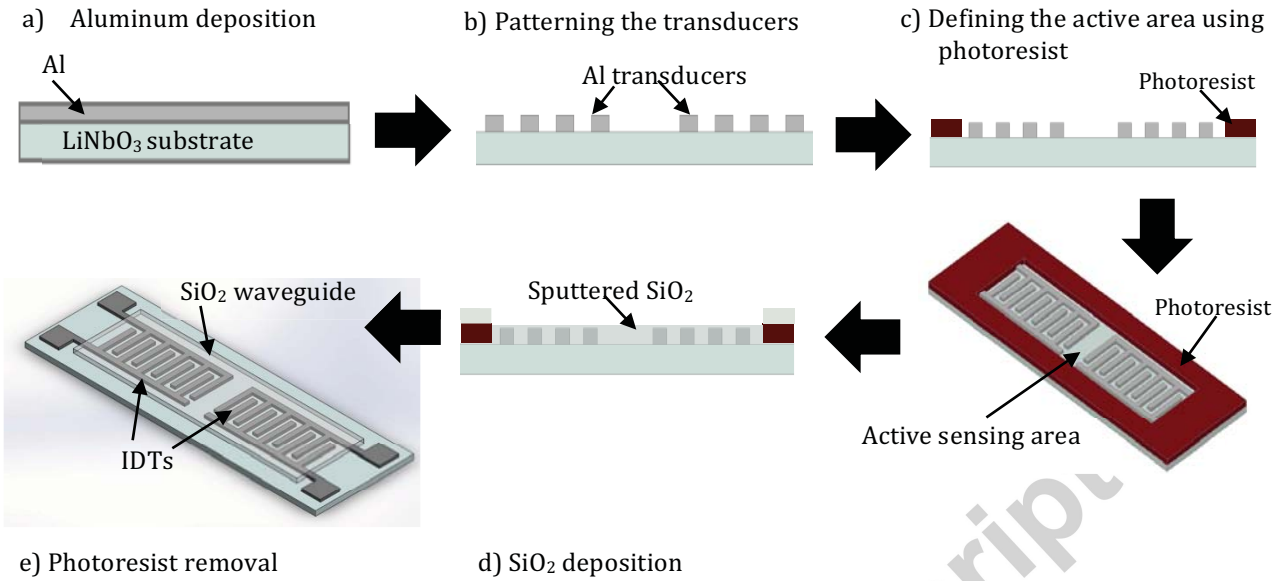

Fig. 1. Shear Horizontal Surface Acoustic Wave device with SiO_2 nanoparticles waveguide fabrication flow.(a) Aluminium deposition using thermal evaporation, (b) Patterning the Al transducers using lithography, (c) defining the active area using photoresist (d) SiO2 deposition using RF sputtering (d) Patterning the SiO2 layer using lift-off process

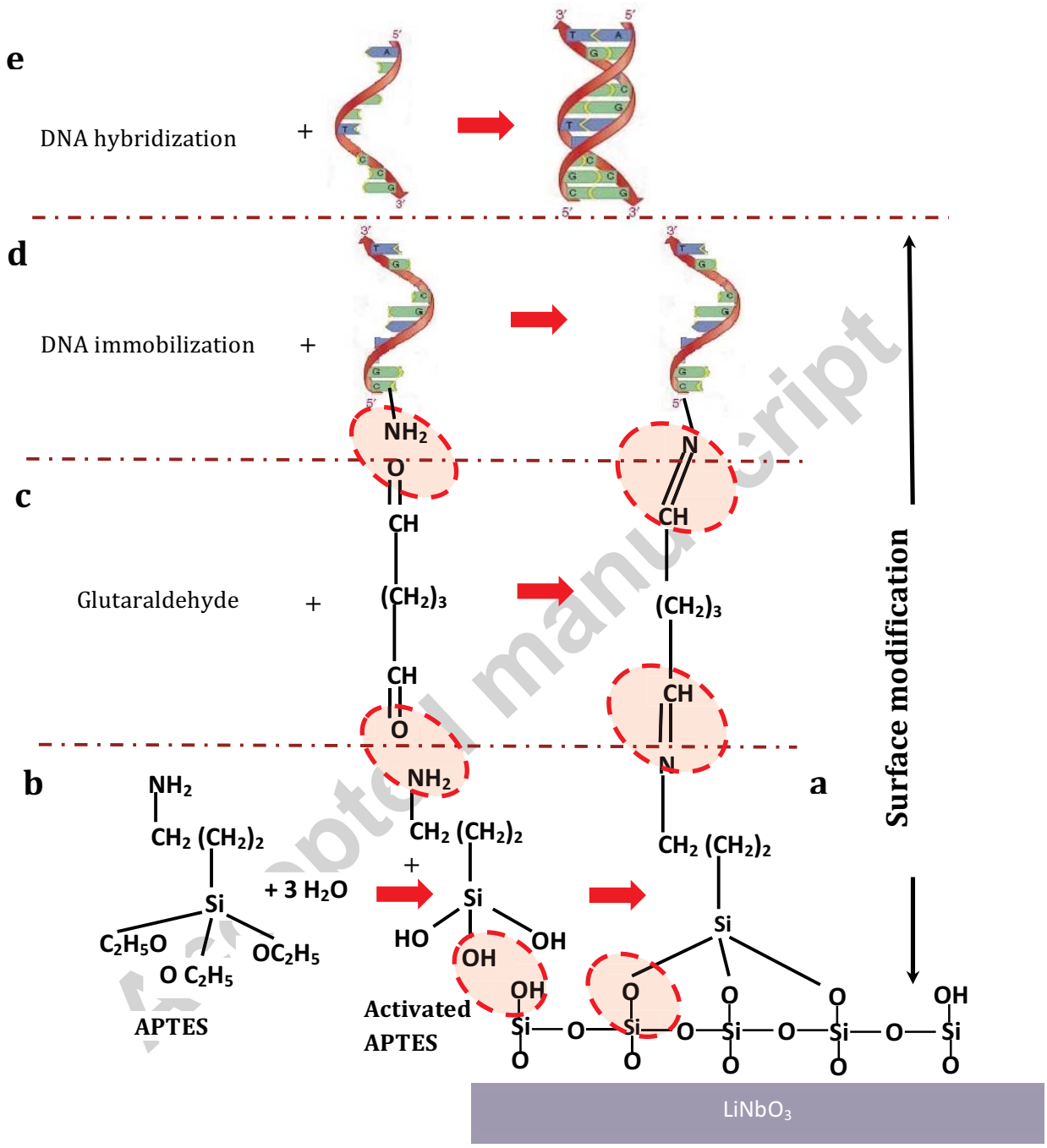

Fig. 2. The surface functionalization process including the surface modification steps from (a) SiO_2 deposition, (b) APTES, (c) glutaraldehyde to (d) probe DNA immobilization processes and (e) DNA hybridization process on $LiNbO_3$ substrate.

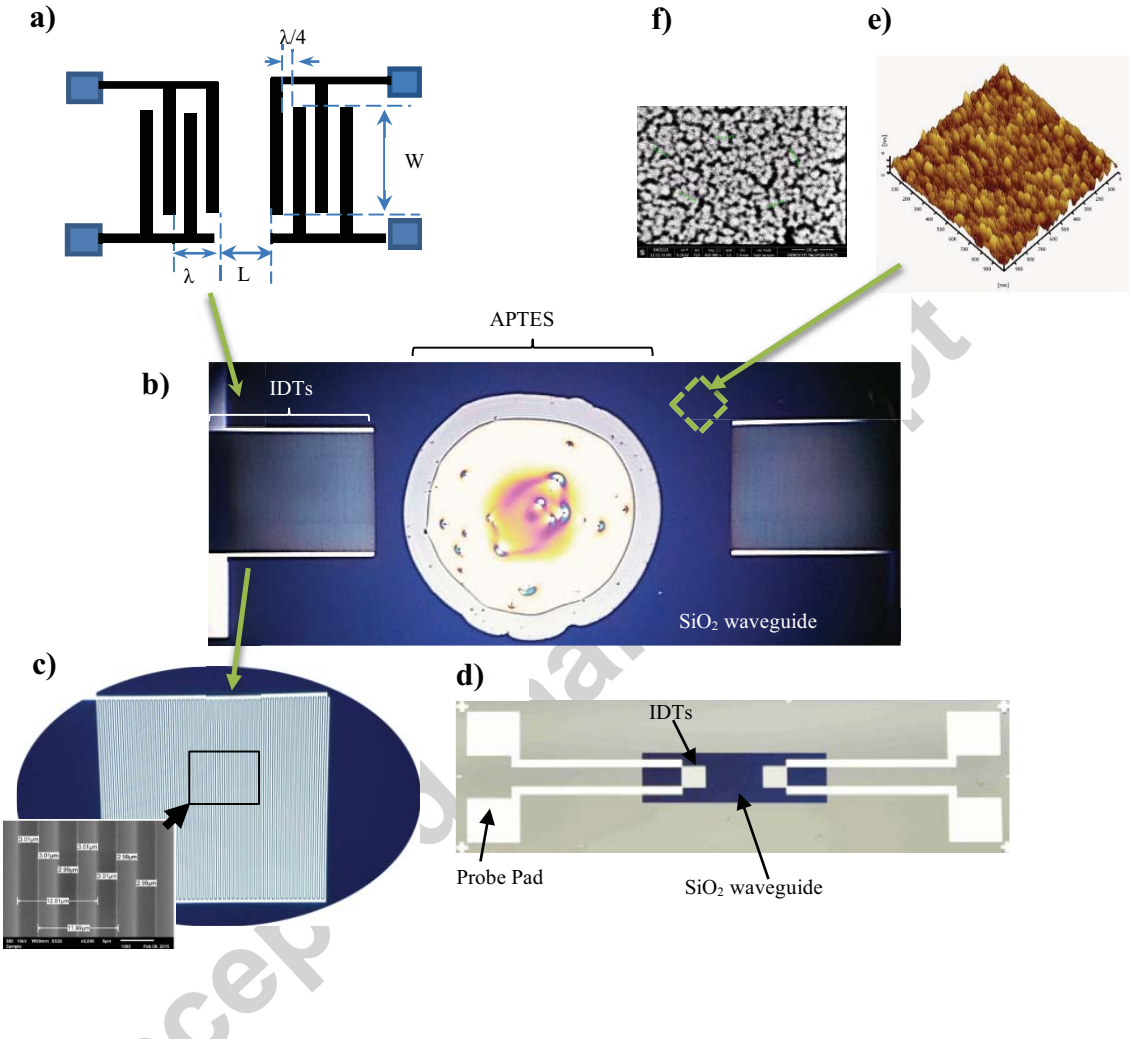

Fig. 3. SHSAW biosensor with SiO_2 nanoparticles waveguide. Clockwise from top left (a) The IDT design parameters (b) Microscope image of the SHSAW fabricated biosensor for *E. coli* O157:H7 detection with APTES. (c) HPM and SEM images of the IDTs. (d) Microscope image of the whole SHSAW biosensor and probe pads. (e) AFM image of deposited SiO_2 layer. (f)FESEM image of the SiO_2 nanoparticles at 5 kV with 800,000 magnification.

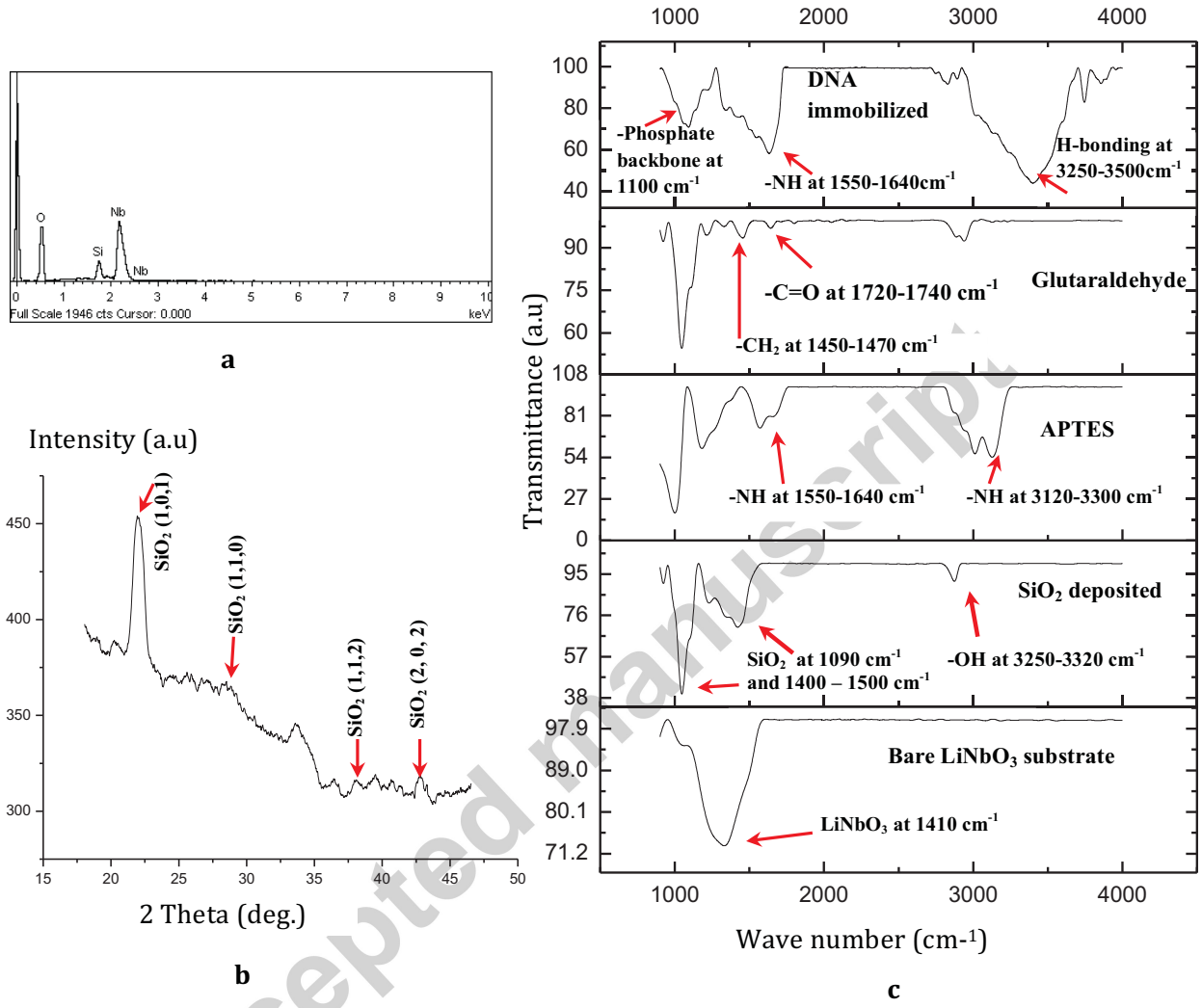

Fig. 4. Affirmation of surface functionalization layers: (a) EDX spectrum upon SiO_2 deposition. (b) SiO_2 compound confirmation by XRD. (c) Infrared spectrum scanning by FTIR upon every layer of surface modification process.

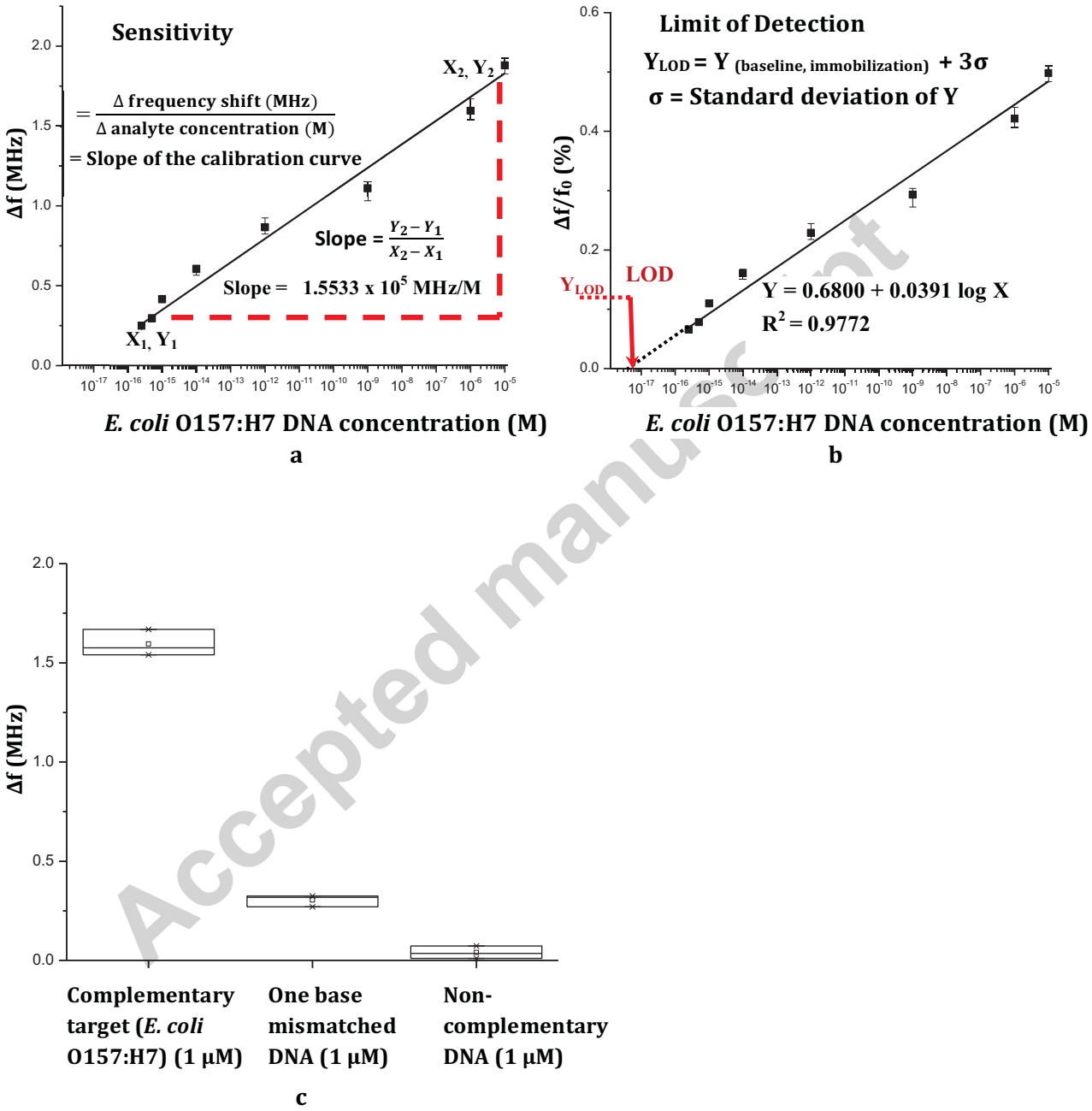

Fig. 5. Analytical performance of SiO_2 nanoparticles waveguide SHSAW biosensor: (a) Frequency shift response curve with different concentrations of *E. coli* O157:H7 DNA. (b) Calibration curve of the relative change in frequency shift according to different concentrations of *E. coli* O157:H7 DNA, display limit of detection (LOD). (c) Hybridization specificity demonstrated by the frequency shift of the complementary, one base mismatched and non-complementary DNA sequences.